Effects of persistence time and Au catalyst on the morphology and optical properties of ZnO micro/nanostructures

Zohreh Negintaji[1], *Abdollah Mortezaali*[1], *Amin Torabi Jahromi*[2], *Elham Yousefi*[3] ✉

[1]*Department of Physics, Al-Zahra University, Vanak, Tehran, Iran*
[2]*Electrical Engineering Department, Persian Gulf University of Bushehr, Bushehr 7516913817, Iran*
[3]*Faculty of Science, Persian Gulf University of Bushehr, Bushehr 7516913817, Iran*
✉ *E-mail: elhamyousefi@stu.yazd.ac.ir*

Published in Micro & Nano Letters; Received on 1st August 2018; Revised on 23rd October 2018; Accepted on 7th December 2018

Zinc oxide (ZnO) micro and nanostructures were synthesised on a quartz substrate by the carbothermal evaporation method. The thin layers of gold were used as a catalyst and syntheses were carried out at different persistence time. Characterisation of the layer was conducted in order to study the effect of persistence time on morphology and crystal structure and optical properties of the fabricated ZnO nanostructures. The samples were characterised by scanning electron microscopy, X-ray diffraction (XRD) and UV–vis spectrophotometry which were performed to investigate the optical properties of the fabricated ZnO layer. The XRD spectrum clearly shows that the structure is in a hexagonal wurtzite phase. Optical properties of ZnO micro and nanostructures were evaluated from transmittance data using the method proposed by Swanepoel (in the regions $\lambda = 200$–900 nm). The study's results indicate that increasing the persistence time as well as decreasing the size of ZnO nanostructures enhances the optical bandgap to about 3.46 eV. To the best of this work's knowledge, this is the first report on the study of the correlation of optical properties obtained by Swanepoel method and morphology of ZnO nanostructures.

1. Introduction: Zinc oxide (ZnO) is one of the most important optoelectronic material with a wide and direct bandgap of 3.37 eV and a large exciton binding energy of 60 meV at room temperature. There has been a lot of interest in growing ZnO nanostructures especially nanowires, nanotubes, nanocombs, nanorings, and nanorods nanoclips motivated by their remarkable physical and chemical properties and the potential applications as nanoscale electronic, photonic, field emission, sensing and energy conversion devices, and chemical and gas sensor devices, solar electrical energy converters [1–8]. Therefore, preparation of one-dimensional nanostructures and investigation of their optical properties have attracted much attention.

Several fabrication techniques have been explored. The most popular one was the vapour transport and deposition [9]. In this technique, there are two main growth mechanisms: vapour–solid (VS) and vapour–liquid–solid (VLS) [10, 11]. Growth process occurs through a VLS mechanism on substrate coated with a catalyst. Owing to the constraints that originated from liquid phase catalyst nanoparticles, the VLS mechanism seldom leads to the formation of complex structures beyond one-dimensional nanowires and nanorods, where the VS mechanism is the driving force [12]. The VLS mechanism has the advantages of a high aspect ratio, low-cost production, geometric control and a large area deposition compared to the growth method.

Here, the effects of catalyst and persistence time on morphology, structure and optical properties of ZnO micro and nanostructures have been investigated. The optical properties of ZnO nano/microstructures are investigated through transmittance spectra obtained via spectrophotometry (Carry500). The experimental data are collected in UV–vis and near-infrared ranges ($\lambda = 200$–900 nm). From the transmittance spectra, the refractive index ($n(\lambda)$), thickness (t) and absorption index ($\alpha(\lambda)$) of the ZnO nanostructures are calculated using the Swanepoel method and the optical bandgap (E_g) is calculated from $\alpha(\lambda)$ [13]. Consequently, a good comparison on obtained optical results related to different structures is performed.

2. Experimental details: In this Letter, the traditional carbothermal evaporation method is used for the synthesis of the ZnO micro and nanostructures. Deposition was carried out in a conventional horizontal tube (150 cm long with a 4 cm diameter) which was surrounded by a cylindrical controllable furnace. A borosilicate tube is used as a deposition chamber. Heating of furnace creates a temperature gradient along the chamber [14]. The precursor is a mixture of commercial ZnO (Aldrich, purity>99.9%) and graphite (Aldrich, purity>99.9%) with weight ratio of 1:1. The powder mixture was placed in the centre of the deposition tube and quartz is used as substrate. For deposition, precursor and substrate are located at a predetermined position (at ∼9.5–10 cm from the centre of the deposition tube), according to the special temperature, inside the chamber under a constant flow of N_2 gas (60 sccm). In this work, the temperature of source materials is adjusted at 1050°C and temperature of substrate is kept at ∼900°C [14, 15]. The system employed for the synthesis of the ZnO micro and nanostructures is illustrated schematically in Fig. 1.

The experiment is repeated for four different deposition timings: 15, 30, 60 and 90 min. The deposited products are characterised by scanning electron microscopy (SEM) (Philips XL30) that is equipped with energy dispersive X-ray spectrometer (EDS). The crystal structure and dominant crystal phase of layer was also examined by the X-ray diffraction (XRD) method.

3. Effect of persistence time: After the furnace temperature reaches to a preset temperature, some time periods are considered for the temperature to stay steady, e.g. 15, 30 or 60 min. After this period (i.e. persistent time) the oven starts to cool down to the environment temperature. Persistence time is an effective parameter on the nanorod diameter as well as the areal density which has been less focused upon in the literature. Fig. 2 shows the SEM micrographs of samples grown on quartz substrates with 15, 30 and 60 min persistence time whereas other growth conditions are kept the same. It can be seen that when the persistence time increases, diameter and density of the rods decrease. This shows that the rate of re-evaporation has proceeded the rate of deposition as the nanoneedles remain on hexagonal bases.

4. Effect of catalyst layer: To investigate the role of catalyst layer on the growth of ZnO wires, the Au droplets which reach

doi: 10.1049/mnl.2018.5440

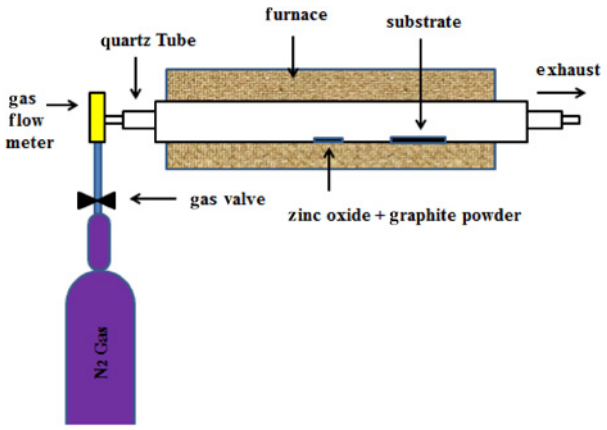

Fig. 1 *Schematic diagram of the system employed for the synthesis of the ZnO micro and nanostructures*

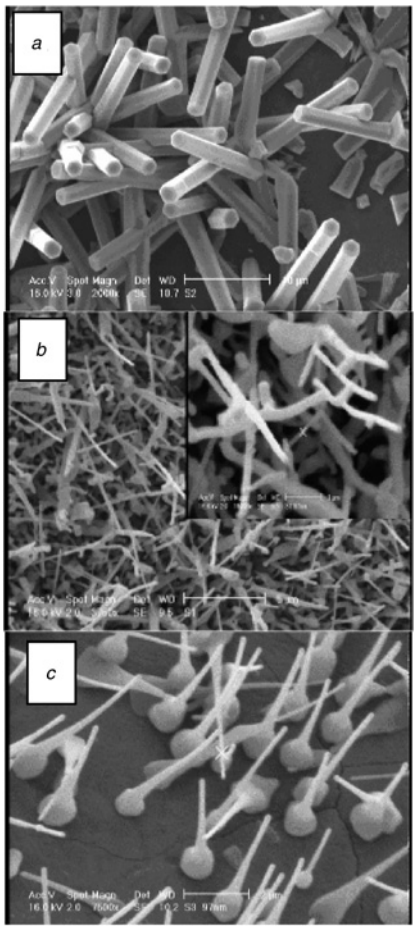

Fig. 2 *SEM images of different ZnO micro and nanostructures obtained at different persistence time on quartz substrates*
a Microstructures at 15 min
b ZnO nanowires at 30 min and
c ZnO nanotips at 60 min

supersaturation were sputtered on quartz substrates. After annealing in 600°C for 1 h, Au islands are formed that act as nucleus for nanowires' growth [16, 17]. Nitrogen gas is used as the carrier gas. There is no discussion on the porosity formation in this Letter. It is worth noting that the experiments were mostly focused on the effect of the persistent time and gold catalyst on the structures and properties of the micro–nanostructures of ZnO.

When ZnO precipitates out as a wire with attention to growth temperature and evaporation point of Au (2807°C), Au catalyst remains on the surface of the substrate and speeds up the deposition process. Increasing persistence time causes the substrates to be exposed to source vapour for a longer time period. Owing to the continuous islands between Au droplets, nanotips of wires attached to each other and forming a porous structure (Fig. 3). Sharp Au peak in the EDS spectrum shows that during reaction time, Au does not evaporate and catalyses the growth (Fig. 4). Compared to the samples grown on free catalyst substrates, a more uniform distribution of the same structures can be observed here. A typical XRD pattern of the grown nanostructures is depicted in Fig. 5. The XRD confirms that wires are crystalline and the preferred orientation growth is ⟨002⟩. The diffraction peaks can be well-indexed to the ZnO wurtzite-type, hexagonal phase with calculated cell parameters $a = b = 3.25$ and $c = 5.21$ nm consistent with the standard values reported previously for bulk ZnO (space group: P63mc, JPCPDF, Card file No.79-0206, wavelength = 1.78897 Å).

5. Optical properties: Fig. 6 presents the transmittance spectra of ZnO nano/microstructures for four samples with persistence time (a) 15, (b) 30, (c) 30 min (with Au catalyst) and (d) 60 min (without catalyst) and bare quartz substrate. There is strong absorption from the substrate at wavelengths below 270 nm. Comparison study on the transmittance spectra reveals that there is much

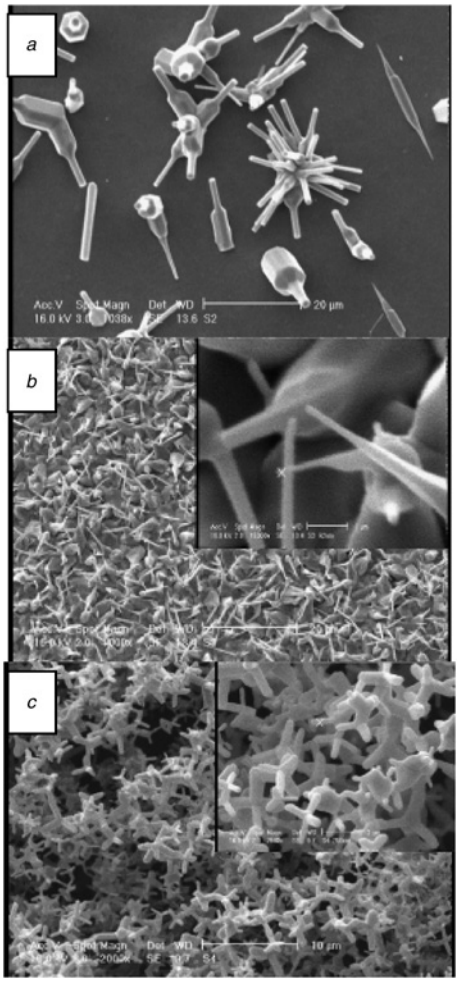

Fig. 3 *SEM images of different ZnO micro and nanostructures obtained at different persistence time on Au coated quartz substrates*
a Nanostructures at 15 min
b ZnO nanotips at 30 min and
c ZnO microstructures at 90 min

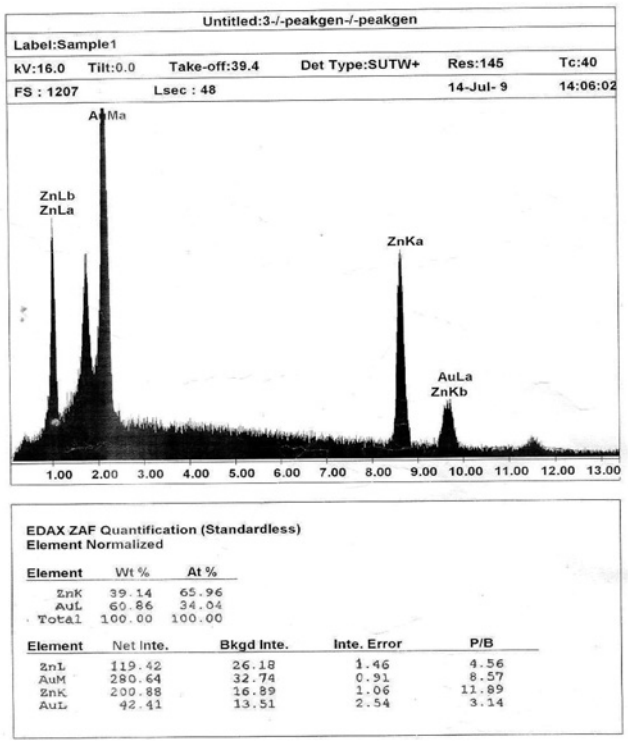

Fig. 4 *EDS analysis of the ZnO nanostructures grown on Au coated quartz*

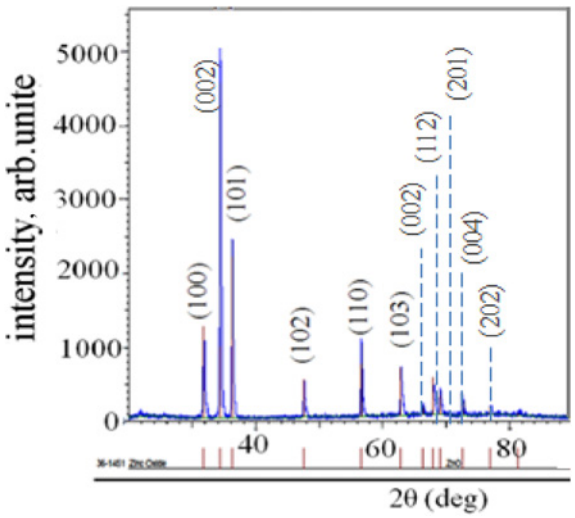

Fig. 5 *XRD pattern of ZnO microstructures with persistence time: 15 min (without catalyst)*

absorption in the ZnO nanostructure layers and it also shows increasing porosity in the samples, according to SEM images, leads to a meaningful increase in transmittance. It is important to note that Au catalyst causes more reflection and has a dominant role in decreasing the refraction index. The refractive index of each sample can be calculated by determination of the following expressions [13]:

$$N = 2n_s \frac{(T_{max} - T_{min})}{T_{max} T_{min}} + \frac{(n_s^2 + 1)}{2} \quad (1)$$

$$n = \left[N + (N^2 - n_s^2)^{1/2}\right]^{1/2} \quad (2)$$

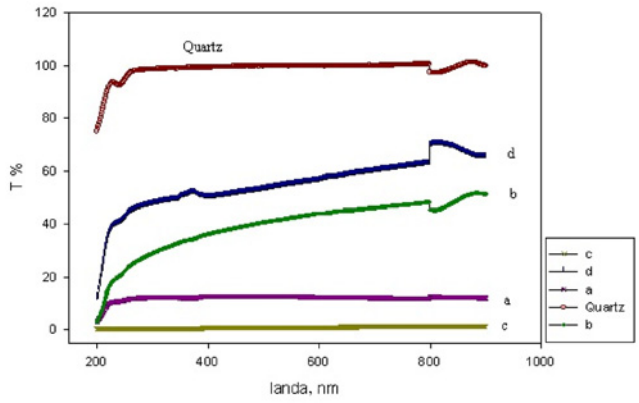

Fig. 6 *Transmittance spectra of ZnO micro/nanostructures for four samples with persistence time*
a 15 min
b 30 min
c 30 min (with Au catalyst) and
d 60 min (without catalyst) and bare quartz substrate

where T_{max} and T_{min} are maximum and minimum temperatures in the transmittance spectrum, respectively. Fig. 7 indicates the values of the refractive index calculated using (2) as a function of the energy for different samples.

The peaks of refractive index spectra occur in the (496–354 nm) range which includes the bandgap absorption edge of ZnO that is located at about 3.37 eV, wavelength of 367 nm. Also, it can be seen that by increasing the porosity, the refractive index decreases. The thickness of thin film nanostructure and absorption index ($\alpha(\lambda)$) can be calculated through the following expressions [13, 18]:

$$t = \frac{\lambda_2 \lambda_1}{2(n(\lambda_2)\lambda_1 - n(\lambda_1)\lambda_2)} \quad (3)$$

$$\alpha = -\frac{1}{t} \mathrm{Ln} \frac{(1-n)(n-n_s)\left((T_{max}/T_{min}) + 1\right)^{1/2}}{(n+1)(n+n_s)\left((T_{max}/T_{min}) - 1\right)^{1/2}} \quad (4)$$

Table 1 includes calculated thicknesses for four samples with persistence time (a) 15, (b) 30, (d) 60 min (without catalyst) and

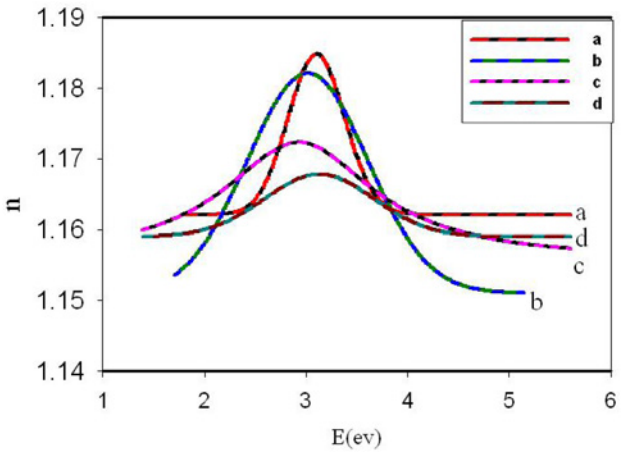

Fig. 7 *Refractive index (n) of the ZnO micro/nanostructures for four samples with persistence time*
a 15 min
b 30 min
c 30 min with Au catalyst and
d 60 min (without catalyst) as a function of the energy (E)

doi: 10.1049/mnl.2018.5440

Table 1 Thickness of four samples with persistence time: (a) 15, (b) 30, (c) 30 min (with Au catalyst) and (d) 60 min (without catalyst)

Sample	a	b	c	d
t, nm	2309.17	978.54	983.0	879.6

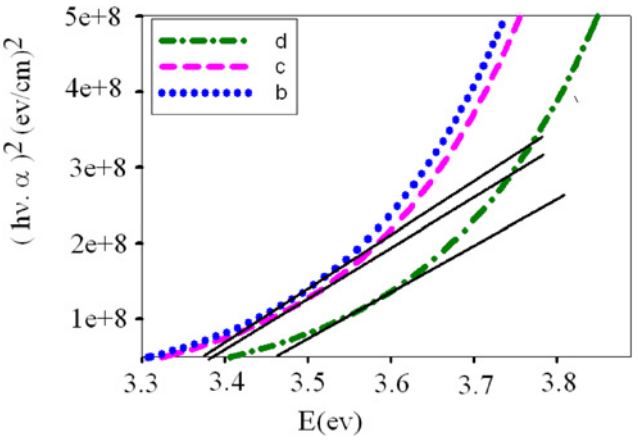

Fig. 8 *Plot of $(h\nu\alpha)^2$ versus $h\nu$ for samples (b) 30 min, (c) 30 min (with catalyst) and (d)60 min (without catalyst). The optical bandgap is given by the intersection of the linear section of the $(h\nu\alpha)^2$ – curve with the $h\nu$ axis (solid lines)*

(c) 30 min (with Au catalyst). The energy gap (E_g) is estimated by assuming a direct transition between valence and conduction bands with this expression [19]

$$\alpha h\nu = K\left(h\nu - E_g\right)^{1/2}, \tag{5}$$

where K is a constant, E_g is the energy gap which is determined by extrapolating the straight line portion of the spectra to $\alpha h\nu = 0$. From these drawings, the optical energy gaps are deduced 3.37, 3.38 and 3.46 eV for samples (b)–(d), respectively, which are presented in Fig. 8. The bandgap energy variation may be related by the degree of non-stoichiometry in ZnO (because of oxygen vacancies) and increasing in its value of sample (d) which can be attributed the Au catalysed absorption of oxygen throughout the sample that produces a more nearly stoichiometric ZnO nanostructure [18–22].

6. Conclusion: In this Letter, it is illustrated that increasing the persistence time leads to the high rate of re-evaporation. It is also practically showed the catalyst layer affects the diameter of micro and nanowires as well as their density. XRD results demonstrate that micro/nanostructures have the ZnO hexagonal wurtzite structure. Swanepoel method is employed to calculate the refractive index as a function of photon energy. The refractive index of ZnO micro/nanostructures has increased by increasing the size of structure and the reduction in porosity but the optical bandgap of ZnO nanostructures was found to increase from 3.37, 3.38 and 3.46 eV by decreasing the size of the nanostructure and increasing the persistence time.

7 References

[1] Wang M., Li A.-D, Kong J.-Z, *ET AL.*: 'Fabrication and characterization of ZnO nano-clips by polyol-mediated process', *Nanoscale Res. Lett.*, 2018, **13**, (47), pp. 1–8

[2] Chae H.U., Park Y-J., Kim H-S.: 'High-speed growth of ZnO nanorods in preheating condition using microwave-assisted growth method', *J. Nanosci. Nanotechnol.*, 2018, **18**, pp. 2041–2044

[3] Laurenti M., Cauda V.: 'ZnO nanostructures for tissue engineering application', *Nanomaterials*, 2017, **7**, (11), p. 374

[4] Cao J., Wu B., Chen R., *ET AL.*: 'Efficient, hysteresis-free, and stable perovskite solar cells with ZnO as electron-transport layer: effect of surface passivation', *Adv. Mater.*, 2018, **30**, p. 1705596

[5] Zhang Y.: 'ZnO nanostructures: fabrication and application' (Royal Society of Chemistry, London, UK, 2017, 1st edn.)

[6] Bouvet-Marchand A., Graillot A., Volk J., *ET AL.*: 'Design of UV-crosslinked polymetric thin layers for encapsulation of piezoelectric ZnO nanowires for pressure-based fingerprint sensors', *J. Mater. Chem. C*, 2018, **6**, pp. 605–613

[7] Wang H., Xuan-Jie H., Ch Li W.-T., *ET AL.*: 'ZnO nanotubes supported molecularly imprinted polymers arrays as sensing materials for electrochemical detection of dopamine', *Talanta*, 2018, **176**, pp. 573–581

[8] Ghasempour Ardakani A., Pazoki M., Mahdavi S.M., *ET AL.*: 'Ultraviolet photo detectors based on ZnO sheets: the effect of sheet size on properties photo response', *Appl. Surf. Sci.*, 2012, **258**, (13), pp. 5405–5411

[9] Vega N.C., Wallar R., Caram J.P., *ET AL.*: 'Zno nanowire co-growth on SiO_2 and C by carbothermal reduction and vapour advection', *Nanotechnology*, 2012, **23**, p. 275602

[10] Huang Y., Zhang Y., He J., *ET AL.*: 'Fabrication and characterization of ZnO comb-like nanostructures', *Ceram. Int.*, 2006, **32**, pp. 561–566

[11] Wang N., Upmanyu M., Karma A.: 'Phase-field model of vapor–liquid–solid nanowire growth', *Phys. Rev. Mater.*, 2018, **2**, p. 33402

[12] Zhang Z., Wang S.J., Yu T., *ET AL.*: 'Controlling the growth mechanism of ZnO nanowires by selecting catalysts', *J. Phys. Chem. C*, 2007, **111**, pp. 17500–17505

[13] Sanchez-Gonzalez J., Diaz-Parralejo A., Ortiz A.L., *ET AL.*: 'Determination of optical properties in nanostructured thin films using the Swanepoel method', *Appl. Surf. Sci.*, 2006, **252**, pp. 6013–6017

[14] Orvatinia M., Imani R.: 'Temperature effect on structural and electronic properties of zinc oxide nanowires synthesized by carbothermal evaporation method', *Int. J. Nanosci.*, 2012, **11**, pp. 1–9

[15] Imani R., Pazoki M., Boschloo G., *ET AL.*: 'Fabrication of microfiber-nanowire junction arrays of ZnO/SnO_2 composite by the carbothermal evaporation method', *Nanomater. Nanotechnol.*, 2014, **4**, p. 211

[16] Dalal S.H., Baptista D.L., Teo K.B.K., *ET AL.*: 'Control label growth of vertically aligned zinc oxide nanowires using vapour deposition', *Nanotechnology.*, 2006, **17**, (19), pp. 4811–4818

[17] Orvatinia M., Imani R.: 'Effect of catalyst layer on morphology and optical properties of zinc-oxide nanostructures fabricated by carbothermal evoporation method', *IET Micro Nano Lett.*, 2011, **6**, pp. 650–655

[18] Grigoryev L.V., Kulakov S.V., Nefedov V.G., *ET AL.*: 'Optcal and photoelectrical properties of nanostructured thin ZnO films for UV-sensors', *J. Phys.: Conf. Ser.*, 2017, **857**, p. 012011

[19] Eshaghi A., Aghaei A.A.: 'Determination of optical properties in nanostructured TiO_2 thin film fabricated by electron beam physical vapor deposition', *J. Opt. Technol.*, 2016, **83**, pp. 26–29

[20] Periasamy C., Prakash R., Chakrabarti P.: 'Effect of post annealing on structural and optical properties of ZnO thin films deposited by vacuum coating technique', *J. Mater. Sci., Mater. Electron.*, 2010, **21**, pp. 309–315

[21] Jayasinghe R.C., Perera A.G.U., Zhu H., *ET AL.*: 'Optical properties of nanostructured TiO_2 thin films and their application as antireflection coatings on infrared detectors', *Opt. Lett.*, 2012, **37**, pp. 4302–4304

[22] Marinov G., Vasileva M., Strijkova V., *ET AL.*: 'Optical properties of ZnO thin films deposited by the method of electrospray', *Bulg. Chem. Commun.*, 2016, **48**, pp. 188–192